European Journal of Medicinal Chemistry 103 (2015) 539–550

Contents lists available at ScienceDirect

European Journal of Medicinal Chemistry

journal homepage: http://www.elsevier.com/locate/ejmech

Research paper

An integrated approach for discovery of highly potent and selective Mnk inhibitors: Screening, synthesis and SAR analysis

Theodosia Teo, Yuchao Yang, Mingfeng Yu, Sunita K.C. Basnet, Todd Gillam, Jinqiang Hou, Raffaella M. Schmid, Malika Kumarasiri, Sarah Diab, Hugo Albrecht, Matthew J. Sykes, Shudong Wang*

Center for Drug Discovery and Development, Sansom Institute for Health Research, Center for Cancer Biology, and School of Pharmacy and Medical Sciences, University of South Australia, Adelaide, South Australia 5001, Australia

ARTICLE INFO

Article history:
Received 11 September 2014
Received in revised form
7 October 2014
Accepted 5 September 2015
Available online 9 September 2015

Keywords:
CGP57380
Eukaryotic initiation factor 4E
Mnk inhibitors
Structure-activity relationship
Thieno[2,3-*d*]pyrimidine
Virtual screening

ABSTRACT

Deregulation of protein synthesis is a common event in cancer. As MAPK-interacting kinases (Mnks) play critical roles in regulation of protein synthesis, they have emerged as novel anti-cancer targets. Mnks phosphorylate eukaryotic initiation factor 4E (eIF4E) and promote eIF4E-mediated oncogenic activity. Given that the kinase activity of Mnks is essential for oncogenesis but is dispensable for normal development, the discovery of potent and selective pharmacological Mnk inhibitors provides pharmacological target validation and offers a new strategy for cancer treatment. Herein, comprehensive *in silico* screening approaches were deployed, and three thieno[2,3-*d*]pyrimidine and pyrazolo[3,4-*d*]pyrimidine derivatives were identified as hit compounds. Further chemical modification of thieno[2,3-*d*]pyrimidine derivative **3** has given rise to a series of highly potent Mnk2 inhibitors that could be potential leads for the treatment of acute myeloid leukemia.

1. Introduction

Dysregulation of cellular translational machinery is a hallmark of cancer [1–3]. Translational initiation is a key rate-limiting step for protein synthesis and is involved in the assembly of eukaryotic initiation factor 4F (eIF4F), including eIF4A RNA helicase, eIF4G scaffold protein and eIF4E cap-binding factor. Binding of eIF4E to eIF4G assists in the recruitment of mRNA on the 40S subunit [4]. Given that the rate of translation is controlled by the availability of eIF4E in cells, eIF4E is thus considered as the key regulator for cap-dependent mRNA translation [5,6].

The oncogenic role of eIF4E has been confirmed with a mouse lymphoma model [7,8]. Activation of eIF4E *via* phosphorylation by the human mitogen-activated protein kinase (MAPK)-interacting kinases (Mnks) [9] repressed apoptosis and engendered tumor formation. Consistently, mice in which Ser209 of eIF4E was mutated to Ala were resistant to Pten$^{-/-}$-induced prostate cancer [10], implying the importance of Mnk-mediated phosphorylation for the transformation activity of eIF4E. The tumorigenic effect of Mnks has been further confirmed by Mnk1/2 double knockout Pten$^{-/-}$ mice, which were found to be resistant to lymphogenesis when compared to the parental Pten$^{-/-}$ mice [11]. Importantly, while the activity of Mnks is necessary for eIF4E-mediated tumorigenesis, it is dispensable for normal tissue development [12]. Thus, inhibiting Mnks offers an exciting opportunity for effectively treating cancer with low toxicity.

Despite the increasing understanding of Mnk-related cancer biology, little progress has been made with the discovery of pharmacological Mnk inhibitors. CGP57380, a known inhibitor of Mnks, showed low micromolar cytotoxicity against various cancer cells [3] while targeting many other kinases with low micromolar IC_{50} values [13]. Cercosporamide, a natural product isolated from *Cercosporidium henningsii*, was initially identified as a broad-spectrum anti-fungal agent [14]. It was only recently discovered that cercosporamide is also a potent Mnk1/2 inhibitor with nanomolar IC_{50} values [15]. Cercosporamide was the first Mnk inhibitor to show *in vivo* anti-tumor efficacy in human xenograft tumor models, and it effectively blocked eIF4E phosphorylation at Ser209, suppressed cancer cell proliferation and led to induction of apoptosis. More recently, we have identified a series of 5-(2-(phenylamino)

* Corresponding author.
E-mail address: shudong.wang@unisa.edu.au (S. Wang).

http://dx.doi.org/10.1016/j.ejmech.2015.09.008
0223-5234/

pyrimidin-4-yl)thiazole-2(3*H*)-one derivatives as potent Mnk2 inhibitors using an analog-based drug design approach [16]. Two compounds were tested against a panel of cancer cell lines, and the results revealed the cell-specific effect of Mnk inhibition. Our study also suggested that Mnk2 inhibitors were capable of reducing the level of anti-apoptotic protein myeloid cell leukemia-1 (Mcl-1), and of inducing apoptosis in MV4-11 acute myeloid leukemia (AML) cells. However, all known Mnk inhibitors target other kinases [13,15], rendering the discovery of potent and selective Mnk inhibitors challenging. Achieving mono- and dual-specific Mnk inhibition is essential to understand the biological relevance and clinical impacts of individual Mnk as most biological studies reported previously were based on the non-selective molecules CGP57380 and cercosporamide.

Structure-based screening has become a prevalent approach in the discovery of small-molecule therapeutics after the successful identification of inhibitors for a number of targets, including FK506 binding proteins, trihydroxynaphthalene reductase, serine protease factor Xa, and v-raf murine sarcoma viral oncogene homolog B1 [17,47–50]. The uniqueness of Mnks is highlighted by two structural elements in the C-terminal lobe, *i.e.* a DFD-motif that replaces the common DFG-motif in other kinases, and three insertions that are exclusively found in Mnks [5,18,19]. Furthermore, this DFD-motif adopts an unusual DFD-out conformation, in which the Phe residue points into the ATP-binding pocket. Such an auto-inhibitory conformation prevents the accessibility of ATP to the binding pocket, and exposes an additional hydrophobic site [20].

There are currently three crystal structures of Mnk2, including apo (PDB ID code: 2AC3) and D228G mutant (PDB ID code: 2AC5) forms as well as Mnk2D228G in complex with staurosporine (PDB ID code: 2HW7) in the Protein Data Bank (PDB). In contrast, only one apo Mnk1 crystal structure (PDB ID code: 2HW6) is available. Staurosporine is a highly potent multi-kinase inhibitor widely used as a chemical probe in diverse protein kinase studies [20]. Closer investigation of the Mnk2D228G-staurosporine complex using docking methods showed that the rigid planar polycyclic ring system of staurosporine lies in a flat orientation in the ATP-binding pocket and the lactam ring forms a total of two hydrogen bonds with the Glu160 and Met162 residues in the hinge region [5]. Such an observation is consistent with the results obtained from a previous study, in which different docking methods were used to replicate the data [21]. Notably, the gatekeeper residue Phe159 in Mnk2 may assist in the formation of favorable hydrophobic interactions with the polycyclic ring system of staurosporine, possibly stabilizing the overall protein-ligand complex [3]. Given that the only crystal structure of Mnk1 adopts the DFD-out conformation, attempts to dock small-molecule Mnk inhibitors into Mnk1 have been hindered. In contrast, crystallographic analysis of the Mnk2D228G-staurosporine complex, where Mnk2 exists in both DFG/D-in and -out conformations, provides a potentially valuable source of structural information for the design of selective Mnk2 inhibitors.

The current study aimed to discover Mnk inhibitors using protein structure-guided and ligand-based screening approaches. Based on chemical structural features of hits identified *in silico*, a series of hit-derived compounds was designed, synthesized and evaluated using human AML cell lines. A number of compounds exhibited improved efficacy and selectivity towards Mnk2. In-house established Mnk1 kinase assays also showed that some of the compounds are potent Mnk1 inhibitors. Clearly, there are distinct roles in the regulation by MAPKs and in basal activity between Mnk1 and Mnk2, despite their high structural similarity [9,22–24]. Mnk1 is activated by Erk and p38 kinases in response to mitogens and stress, respectively, but Mnk2 is only phosphorylated *via* the Erk pathway. Mnk2 does not respond to the stimuli-induced p38 activation, and therefore may have a different role in inducing cytokine production and regulating cytokine responses in comparison with Mnk1 [25]. As no specific Mnk1 or Mnk2 inhibitors exists, our first-in-class selective inhibitors of Mnk1/2 will be powerful pharmacological tools in distinguishing Mnk1/2-related biology, pharmacology and drug discovery.

2. Results and discussion

2.1. Validation of computational approaches

To assess the reproducibility of bioactive conformations by the 3D conformation generator OMEGA, the co-crystallized staurosporine in the Mnk2 protein structure (PDB ID code: 2HW7) was selected as the starting point. The co-crystallized conformation was extracted and aligned with the conformations generated by OMEGA using vROCS. A good correlation was observed between the highest scoring OMEGA generated conformation and the co-crystallized staurosporine conformation (Fig. 1A), as indicated by a TanimotoCombo score of 1.47. All output conformations produced by OMEGA were of interest nonetheless, as it is known that the

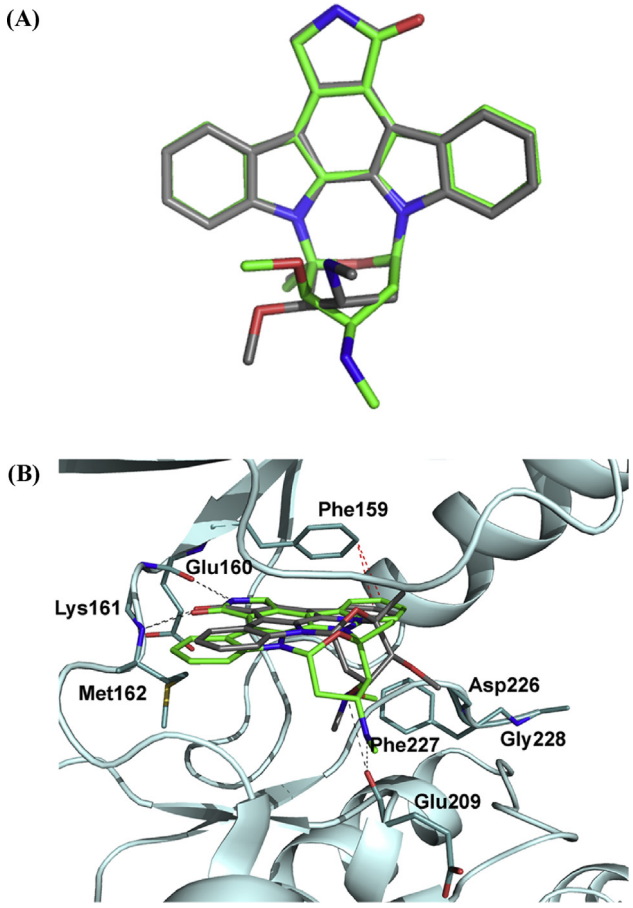

Fig. 1. Validation of computational approaches. (A) Overlay of two staurosporine poses obtained from the co-crystallized structure with Mnk2 (PDB ID code: 2HW7) (green sticks) and OMEGA-constructed method (black sticks), respectively. The figure was generated using VIDA v4.0.3. (B) Docking of the co-crystallized staurosporine pose (green sticks) and the OMEGA-constructed pose (black sticks) against the Mnk2 receptor (PDB ID code: 2HW7). Mnk2 is shown as cyan ribbons. The Phe gatekeeper, hinge residues and DFD motif are in capped sticks. Hydrogen bonds are shown as black dashed lines. $\pi-\pi$ stacking interactions between the aromatic rings are shown as red dashed lines. The figure was generated using Pymol v1.6.

ability to generate an ensemble of conformations encapsulating the bioactive conformation impacts the identification of the correct binding poses [26]. Therefore, the maximum number of output conformations was varied (50, 100 and 200) and applied to the molecules of a previously built in-house control database, including the three known Mnk inhibitors (see Experimental Section 4.1.1). An exploratory docking of these generated conformer sets against the Mnk2 receptor using the X-ray crystal structure (PDB ID code: 2HW7) revealed that the ranking of the active molecules were either unchanged by the introduction of a larger number of conformations or degraded (Table S1). Hence, for computational efficiency, a maximum number of 50 conformers was used for the subsequent screening.

The ability of OEDocking [27] to identify accurate binding poses was assessed by two approaches. The first method assessed its ability to reproduce the co-crystallized staurosporine pose (Fig. 1B). The root mean square deviation (rmsd) between the co-crystallized and docked staurosporine poses was only 0.45 Å, providing initial evidence of the applicability of OEDocking in this study. Therefore, the parameter sets used in the initial conformer generation and docking were employed for the Mnk2 screening that followed. In the second approach, the docking results generated by the Mnk2 receptor against the control database were re-assessed to determine the threshold point (in terms of docking score) for retrieving potential Mnk2 hits. Out of the 38 molecules in this database, 7 molecules were identified as actives. Not unexpectedly, CGP052088, a known Mnk inhibitor derived from staurosporine [28], was the top ranked molecule with a docking score of −14.09 (Table S1). This was followed by one of the most active compounds among the hits (JQ12445675), accounting for a docking score of −12.67. Despite the broad distribution of the actives throughout the ranking list, all of the 7 actives were retrieved from the database with a docking score of −6.50 or less. Hence, a threshold score of −6.50 was set to identify potential Mnk2 hits.

2.2. Virtual screening approaches

Fig. 2A depicts the workflow of the virtual screening, including database preparation and filtration followed by the combinatorial *in silico* screening. Initially, the ChemBridge database consisting of 572 K compounds was pre-filtered and the resulting 387 K compounds were converted to 3D conformers using OMEGA (see Experimental Section 4.1.1). The original ionization states of the compounds were retained and the new 3D database generated was subjected to two different approaches to maximize the virtual screening hit rate.

The first approach involved docking of the 3D database against the active site of Mnk2. The 1000 top-scoring compounds were selected for inspection. The ensuing molecules were analyzed for their ability to form interactions with the protein residues known to contribute significantly to Mnk2 binding, in the context of the following criteria: possession of (1) at least one hydrogen bond with the hinge residues (*i.e.* Glu160, Lys161 and Met162), (2) a central aromatic moiety that forms π–π stacking interactions with the gatekeeper Phe159 within a distance of 4 Å or less, and (3) one hydrophobic group pointing towards the hydrophobic region 1 (HR1; formed by residue Phe159) or hydrophobic region 2 (HR2; formed by residues Met162, Gly164, Gly165 and Leu212) [5].

In the second approach, the same 3D database was submitted for ligand-based alignment. CGP57380 and cercosporamide, representing two distinct chemical scaffolds, were selected as queries. The top 200 compounds from each alignment set, ranked according to the TanimotoCombo score [29], were retrieved and re-docked to the Mnk2 receptor to meet the aforementioned criteria. Collectively, these stringent screening criteria successfully filtered out ~97% of molecules, leaving a set of 40 structurally diverse compounds. The drug-like properties and commercial availability of these compounds were considered and 13 candidates were selected and purchased for biological evaluation (Table S2).

2.3. Assessment of Mnk2 inhibitors

The selected 13 candidates were evaluated at concentrations of 1 and 10 μM by employing an Mnk2 biochemical assay (Fig. 2B). CGP57380 was included as a positive control. Candidates that exhibited > 50% inhibitory activity in the assay were further subjected to IC_{50} determination against Mnk1 and Mnk2. CDK2/cyclin A plays a regulatory role during the G1 to S phase transition in cell cycle [30], and inhibition of CDK2 leads to cell arrest in G_1/S phase [31]. Inhibition of Mnk results in down-regulation of cell cycle regulatory proteins including cyclin D causing G_1 cell arrest [3,51–53]. In our recent study, CDK9 inhibition led to the down-regulation of Mnk and the consequent reduction of eIF4E phosphorylation in ovarian cancer cells [32]. To ensure that the biological effects observed are exerted through Mnk inhibition and are not consequences of inhibiting CDK2 and CDK9, the assessment against both CDKs was also carried out for the initial selectivity profile. This procedure eliminated 10 of the 13 hits, yielding a virtual screening hit rate of 23%. The structures and biological activities of the remaining three hit compounds are summarized in Fig. 2B. Hits **1** and **3** (ZINC00132478 and ZINC00098359, respectively) are thieno[2,3-*d*]pyrimidine derivatives while hit **2** (ZINC00450245) shares a pyrazolo[3,4-*d*]pyrimidine scaffold with CGP57380. Hit **3** demonstrated potent Mnk2 inhibitory activity with a K_i value of 0.620 μM, whereas hit **1** showed a modest potency (K_i = 3.430 μM). Both thieno[2,3-*d*]pyrimidine derivatives demonstrated excellent selectivity for Mnk2 over CDK2/A and CDK9/T1 (K_i > 10 μM). Hit **2** was also found to be a potent Mnk2 inhibitor (K_i = 0.523 μM), being comparable to CGP57380; however it also targets CDK2/A and CDK9/T1 (K_i = 3.046 and 7.873 μM, respectively). All hits displayed cytotoxicity with GI_{50} values ranging between 4.95 and 8.81 μM against MV4-11 and MOLM-13 leukemic cell lines.

The importance of adopting the ligand-based alignment method is highlighted when all three hits were shown to be retrieved from this method in the virtual screening study (Table S2). Fig. 2C depicts the molecular shape and chemical feature matches between CGP57380 and hit **3** in a similarity assessment using the TanimotoCombo metric. As indicated by the partial charge density, hit **3** shows chemical features similar to CGP57380. On the basis of the docking study (Fig. 2D), the presence of at least one hydrogen bond with the hinge residue(s) of Mnk2 and the adoption of an appropriate geometry for the π–π stacking interaction with the gatekeeper Phe159 (distance of ≤ 4 Å), are two key parameters as the preliminary filter for selecting hits, which is consistent with our previous proposed models for the optimal Mnk2 ligand binding [3,5]. As this study aimed to identify selective Mnk inhibitors, the thienopyrimidine scaffold, which has a distinctive core structure relative to the known Mnk2 inhibitors, was pursued further for structural optimization.

2.4. Hit optimization, assay validation and structure-activity relationship analysis

To facilitate chemical modifications on the thienopyrimidine core, further exploration of the binding modes of CGP57380 or cercosporamide against Mnk2 was undertaken. Close inspection of the docking models showed that cercosporamide protrudes its acetyl group into a relatively acidic pocket (adjacent to the specific

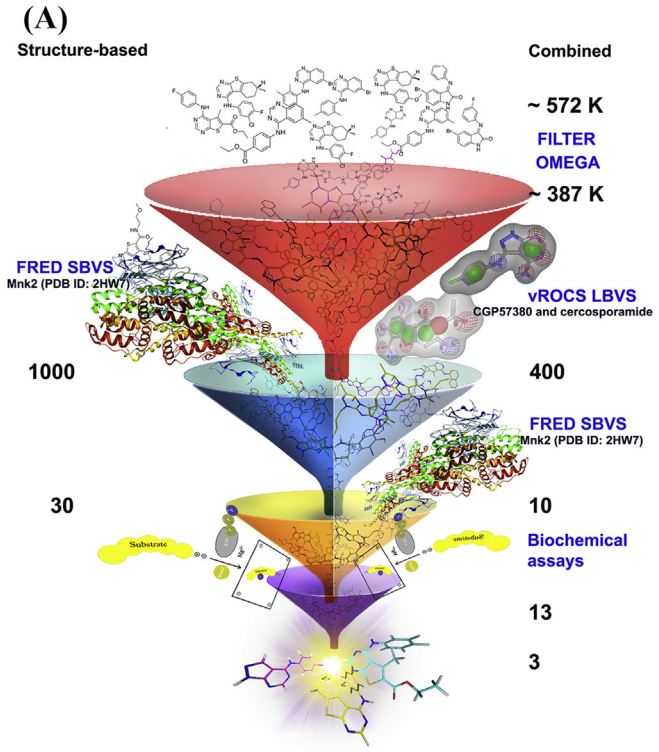

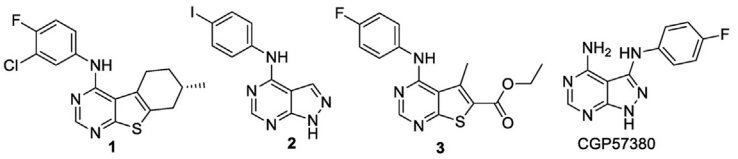

Hit	MW	vROCS alignment	FRED docking			Kinase inhibition K_i (μM)			Cytotoxicity GI_{50} (μM) ± SD	
		Tanimoto Combo	Chemgauss score	No. of H-bonds	π-stacking distance (Å)	Mnk2	CDK2A	CDK9T1	MV4-11	MOLM-13
1	347.84	1.209	-10.895	1	3.55	3.430	>10	>10	5.30 ± 2.18	7.68 ± 1.73
2	337.12	1.315	-9.976	2	3.56	0.523	3.046	7.873	4.95 ± 0.16	6.75 ± 2.02
3	331.37	1.210	-9.577	1	4.00	0.620	>10	>10	5.25 ± 0.44	5.82 ± 2.47
CGP	244.20	2.000	-10.632	2	3.35	0.340	>10	>10	6.89 ± 0.16	8.81 ± 0.80

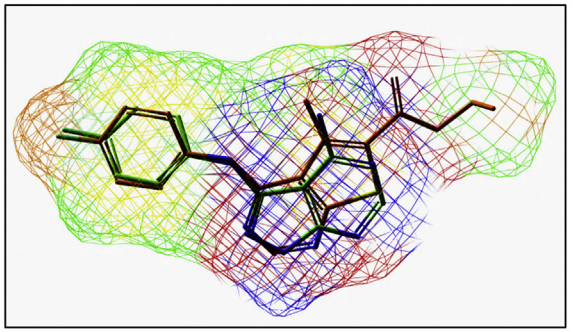

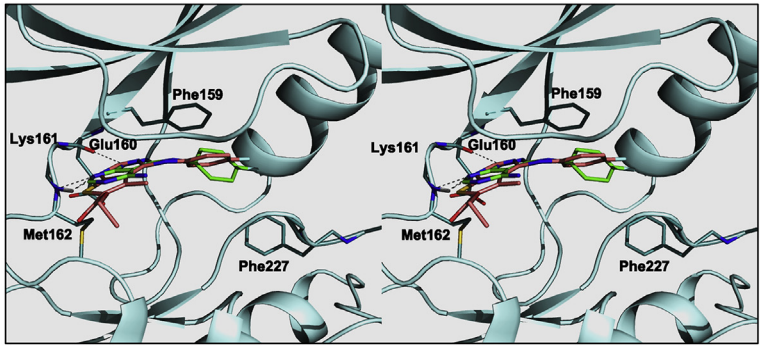

Fig. 2. Cascade screening for Mnk inhibitors. (A) Computational steps including database filtration, conformer generation, docking-based design and ligand-based study were performed using Openeye Scientific Software. SBVS, structure-based virtual screening; LBVS, ligand-based virtual screening. See also Tables S1-2. (B) Chemical structures of the final three hits and their virtual screening and biological evaluation results. Hits **1**–**3** were purchased from Hit2Lead online chemical store that reported to have a compound purity of ≥ 95% by NMR and LC-MS. vROCS alignment result when CGP57380 was used as a query. Number of hydrogen bond interactions with the Mnk2 hinge residues (*i.e.* Glu160, Lys161 and Met162) in the docking analysis using VIDA. Apparent inhibition constants (K_i) were calculated from IC_{50} values and the appropriate K_m (ATP) values for each kinase. The assays were tested by Millipore KinaseProfiler™ services. Cytotoxicity by 72 h resazurin assays. The data given are mean values derived from at least two replicates ± SD. (C) vROCS alignment of hit **3** (orange sticks) shown in the partial charge mesh surface when CGP57380 (green sticks) was used as a query molecule. (D) Proposed binding modes of CGP57380 (green sticks) and hit **3** (orange sticks) against the Mnk2 receptor (PDB ID code: 2HW7). Mnk2 is shown as cyan ribbons. The Phe gatekeeper, hinge residues and DFD motif are in capped sticks. Hydrogen bonds are shown as black dashed lines. The figure was generated using Pymol v1.6.

DFG/D-motif, Fig. 3A) formed by residues Glu92, Glu209, Asn210 and Ile211, which has not been found in the Mnk2 complex with CGP57380 or hit **3**. Given that cercosporamide is the most potent Mnk2 inhibitor [15] among the previously identified compounds, exploitation of this region with an appropriate functionality may confer an increase in potency towards Mnk2.

Analysis of the docking mode of hit **3** in Mnk2 showed that an additional substitution at the *ortho*-position of the aniline ring, in the context of the thienopyrimidine core, might be able to target the pocket to enhance the binding affinity (Fig. 3B). The synthesis of analogs of hit **3**, *i.e.* 4-((4-fluorophenyl)amino)-5-methylthieno[2,3-*d*]pyrimidine-6-carboxylate derivatives, was hence pursued and is outlined in Scheme 1. Compounds **5a**–**c**, **6a**–**c** and **7a**–**e** were assessed for kinase inhibitory potency and selectivity against Mnk1, Mnk2, CDK2/A and CDK9/T1 (Table 1). Our previous work has shown that Mnk2 inhibitors demonstrated tumor cell growth inhibition in a cell-type specific manner, being particularly cytotoxic against MV4-11 cells [16]. Thus, MV4-11, together with MOLM-13 (which are also acute monoblastic leukemia cells, *i.e.* M5 subtype, expressing Fms-like tyrosine kinase 3-internal tandem duplication (FLT3-ITD) mutations as MV4-11) [33], were chosen for the antiproliferative assessment of the compounds.

Profiling of Mnk inhibition involved the two in-house assays, *i.e.* an initial rapid screen using immobilized metal ion affinity particle (IMAP) technology [34] followed by a dose–response analysis adopting the ADP-Glo^{TM} luminescent kinase assay [35]. Validation of the assays was performed by optimizing the concentrations of Mnk1 and Mnk2, eIF4E-derived substrates and ATP (Figure S2). Two well-defined Mnk inhibitors, CGP57380 and cercosporamide, were employed as model inhibitors for the in-house assays and the published IC_{50} values from radio-active kinase assays [13,15] were used as standard references in the current study (Table 1). A 2-fold inhibitory preference of Mnk1 over Mnk2 was previously reported for CGP57380 (IC_{50} values = 0.87 and 1.60 μM for Mnk1 and Mnk2, respectively) [13]. Our data, however, revealed no significant difference in relative potency against the two kinases (K_i = 1.010 and 0.877 μM for Mnk1 and Mnk2, respectively). In contrast, cercosporamide was found to be 6-fold more potent against Mnk2 than Mnk1 (K_i = 0.507 and 0.079 μM for Mnk1 and Mnk2, respectively) in our study, which is in close correlation with the data obtained from the literature [15]. Hence, the established Mnk1 and Mnk2 assays were used to analyze newly synthesized compounds.

A change of substituent on the C6-position of thienopyrimidine in hit **3**, from an ethyl ester to a methyl ester (**5a**, R^1 = H, R^2 = OMe), was found to abolish Mnk2 inhibitory activity, and the same holds true for the cytotoxicity. Additionally, no Mnk1 inhibitory activity was detected in **5a**. Further introduction of a methyl group at the *ortho* position of aniline (**5b**, R^1 = Me, R^2 = OMe) shows no improvement in either kinase activity or cellular potency. Introducing an *o*-isopropoxyl group gives rise to **5c** (R^1 = $OCHMe_2$, R^2 = OMe) with slightly restored Mnk2 activity and cytotoxicity. No inhibition of Mnk1, CDK2/A and CDK9/T1 was observed.

In contrast, conversion of the methyl ester moiety of **5a** into the carboxylic acid group (**6a**, R^1 = H, R^2 = OH) was found to dramatically enhance Mnk2 inhibitory activity, which is more than 3-fold greater in comparison with hit **3**, but has a detrimental effect on cellular activity. However, in comparison with **6a**, the methyl derivative **6b** (R^1 = Me, R^2 = OH) displays a reduced activity against

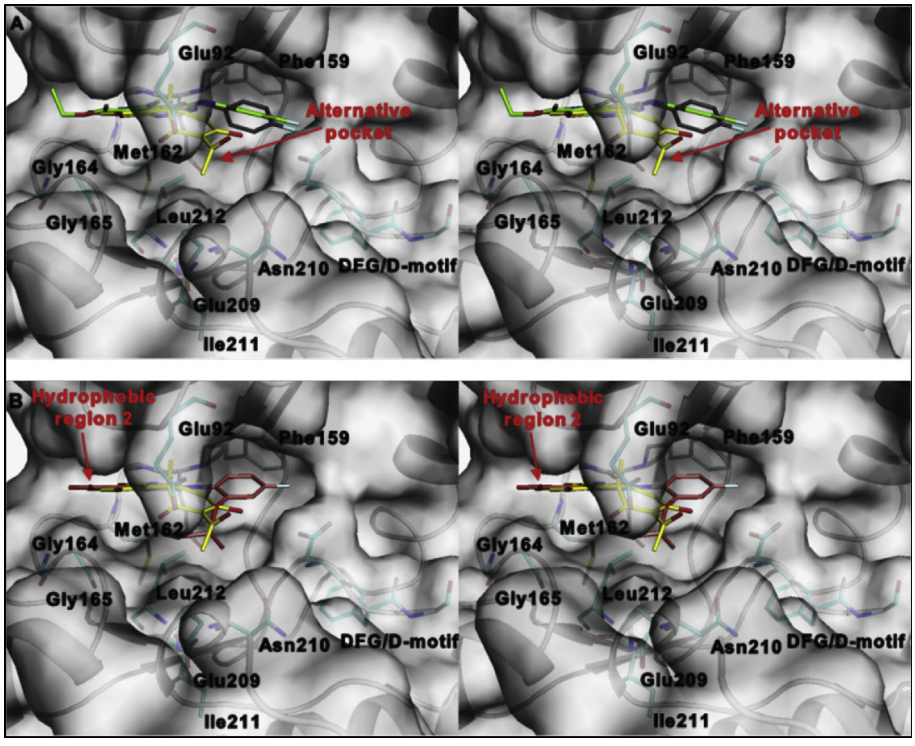

Fig. 3. Stereoview of structures of inhibitors in ATP-binding site of Mnk2. (A) CGP57380 (black sticks) and hit **3** (green sticks) possess a fluoroaniline moiety, in which the aromatic ring is likely to be stabilized by the Phe159 gatekeeper. A pocket (adjacent to the DFG/D-motif, red arrow) formed by residues Glu92, Glu209, Asn210 and Ile211, accommodates the hydrophobic moiety on cercosporamide (yellow sticks), highlighting the importance of assessing to such a pocket for modulating potency. (B) A proposed binding mode of hit **3** against Mnk2 after the introduction of an isopropoxyl group at *o*-position of fluoroaniline (pink sticks). The compound protrudes the isopropoxyl group into the alternative pocket, in in a way similar to that of the cercosporamide (yellow sticks). Docking analysis also revealed a favored C6-carboxamide in the hydrophobic region 2 (formed by residues Met162, Gly164, Gly165 and Leu212). The binding modes were generated by docking the multiple poses to the Mnk2 X-ray structure (PDB ID code: 2HW7) using OEDocking and the pose with best scoring function is presented. The figure is generated using Pymol v1.6.

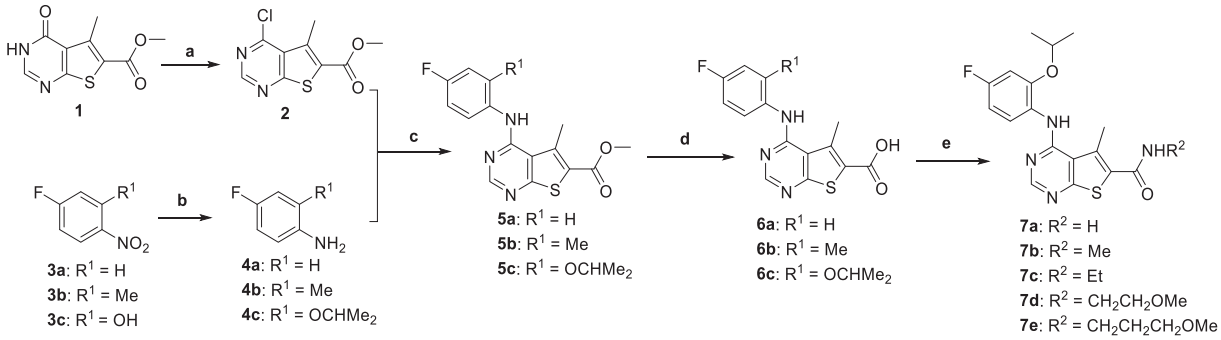

Scheme 1. Synthesis of methyl 4-((4-fluorophenyl)amino)-5-methylthieno[2,3-*d*]pyrimidine-6-carboxylates (5a–c) and their derivatives (6a–c and 7a–e). Reagents and conditions: (a) $SOCl_2$, DMF, reflux, 2 h, 80%; (b) H_2, 10% Pd/C, MeOH, rt, 2–3 h, **4a**: 100%, **4b**: 100%, **4c**: 92%; (c) TsOH·H_2O, 1,4-dioxane, microwave, 150 °C, 0.5 h, **5a**: 18%, **5b**: 32%, **5c**: 79%; (d) For **5a** and **5b**, NaOH, MeOH/THF, 70 °C, 4 h, **6a**: 87%, **6b**: 91%; for **5c**, LiOH, MeOH/THF/H_2O, rt, o/n, **6c**: 67%; (e) appropriate amine, HATU, DIPEA, DMF, rt, o/n, **7a**: 86%, **7b**: 63%, **7c**: 34%, **7d**: 51%, **7e**: 48%.

Table 1
Summary of structure and biological activity.

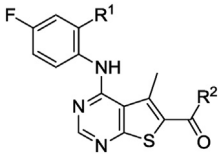

Code	Structure		Kinase inhibition K_i (μM)				72 h GI_{50}[c] (μM) ± SD	
	R^1	R^2	Mnk2[a]	Mnk1[a]	CDK2A[b]	CDK9T1[b]	MV4-11	MOLM-13
CGP57380	–	–	0.877	1.010	>10	>10	6.89 ± 0.16	8.81 ± 0.80
Cercosporamide	–	–	0.079	0.507	–	–	–	–
5a	H	OMe	>10	>10	–	–	78.6 ± 8.01	68.3 ± 5.15
5b	Me	OMe	>10	>10	–	–	88.1 ± 6.94	93.1 ± 9.81
5c	$OCHMe_2$	OMe	4.050	>10	>10	>10	9.38 ± 0.10	4.61 ± 0.36
6a	H	OH	0.164	1.900	–	–	78.3 ± 2.34	79.3 ± 0.08
6b	Me	OH	0.500	>10	–	–	89.4 ± 9.58	>100
6c	$OCHMe_2$	OH	0.068	0.186	>10	>10	7.30 ± 0.75	5.65 ± 0.84
7a	$OCHMe_2$	NH_2	0.110	1.020	>10	>10	6.08 ± 1.99	6.12 ± 0.44
7b	$OCHMe_2$	NHMe	0.018	0.106	>10	>10	5.29 ± 1.89	5.76 ± 1.05
7c	$OCHMe_2$	NHEt	0.018	0.933	>10	>10	8.84 ± 1.58	8.65 ± 1.77
7d	$OCHMe_2$	$NHCH_2CH_2OMe$	0.031	>10	>10	>10	7.44 ± 0.77	7.19 ± 0.08
7e	$OCHMe_2$	$NHCH_2CH_2CH_2OMe$	0.164	0.320	>10	>10	15.3 ± 2.62	50.4 ± 7.40

[a]The kinase assays were developed and conducted in-house. See also Fig. S2. [b]The assays were tested by Merck Millipore. [a,b]The ATP concentrations used in these assays were within 15 μM of K_m. Apparent inhibition constants (K_i) were calculated from IC_{50} values and the appropriate K_m (ATP) values for each kinase. [c]Anti-proliferative activity by 72 h resazurin assays. Data shown are the mean values derived from at least two replicates ± SD.

Mnk2, but is comparable to hit **3**. This compound demonstrates an excellent selectivity for Mnk2 over Mnk1, but has a reduced cellular potency. These results imply that the carboxylic acid may facilitate the interaction with Mnks but give rise to a poor cell-based activity plausibly due to poor permeability. Thus, replacement of the methyl ester of **5c** with the carboxylic acid in **6c** (R^1 = $OCHMe_2$, R^2 = OH) results in a > 50-fold increase in Mnk inhibitory activity. Of note, **6c** has a Mnk2 activity very similar to that of cercosporamide, along with a 2-fold improvement in Mnk1 activity. These findings indicate a balance between the two key substituents R^1 and R^2 need to be achieved for optimal activity. Once again, no CDK inhibition is seen, indicating the anti-proliferative effects exhibited by **6c** on AML cells are derived from the inhibition of Mnks.

Since both satisfactory Mnk inhibitory activity and cytotoxicity were achieved by compound **6c**, the proposed Mnk2-**6c** binding model was analyzed. It reveals a favored C6-carboxamide in the HR2 (formed by residues Met162, Gly164, Gly165 and Leu212, Fig. 3B), suggesting optimization at the C6-position of **6c** may result in further enhancement of activity against Mnk2. Hence, analogs **7a**-**e** were synthesized by amide formation between **6c** and selected amines. As expected, compound **7a** (R^1 = $OCHMe_2$, R^2 = NH_2) shows no improvement in both enzymatic and cellular activity compared to **6c**. A slight increase in the hydrophobicity of **7a**, as shown by compound **7b** bearing an *N*-methyl C6-carboxamide, improves the affinity for both Mnk1 and Mnk2 by ~6-fold. Introduction of a bulkier alkyl substituent into **7a**, *i.e.* **7c** (R^2 = Et) and **7d** (R^2 = CH_2CH_2OMe) retains the Mnk2 activity but reduces Mnk1 inhibition by at least 9-fold. However, in the case of **7e** (R^2 = $CH_2CH_2CH_2OMe$), Mnk2 inhibitory activity decreases whereas the affinity for Mnk1 is restored. In general, Mnk1 activity decreases when the substituent at C6-position becomes bulkier. This trend may be attributed to the structural observation that Mnk1 comprises a more compact ATP-binding pocket when compared with Mnk2 [5]. Taken together, these data suggest the

structural modification at the C6-position plays a pivotal role in governing the kinase activities, particularly for Mnk2.

None of compounds **7a**–**e** are active against CDK2/A and CDK9/T1 (K_i > 10 μM) and show cellular cytotoxicity (GI_{50} = 5.29–8.84 μM) with the exception of **7e** which exhibits lower anti-proliferative activity. As suggested by our previous studies with CDK2 and CDK9 inhibitors [16,36], two hydrogen bond interactions of a given inhibitor with the hinge residues Leu83 of CDK2 (Cys106 in CDK9) followed by a π–π interaction with the gatekeeper Phe80 (Phe103 in CDK9) are required for activity. In contrast, our docking studies of **6c** and **7d** in CDK2 or CDK9 failed to generate any appreciable binding poses (Figure S3). The 1S and 6C-carbonyl of thienopyrimidine seem unable to make any appropriate interaction with the hinge residues.

It is also worth noting that a recent patent application has described a series of thienopyrimidine-based compounds as highly potent Mnk inhibitors [37], which serves as further validation of our discovery strategy. Despite the similar chemical scaffold to the patented structure, the current work has showcased an integrated computational and experimental approach to identify the most potent compound series to date.

3. Conclusions

This report has described the discovery, optimization and characterization of a series of thienopyrimidine-based Mnk inhibitors that possess high potency and selectivity. The *in silico* virtual screening that used an integrated approach of ligand-based and structure-based has led to identification of Mnk2 hits. Further structural optimization of hit **3** by adding an isopropoxyl group at the *ortho*-position of 4-fluoroaniline to occupy a pocket adjacent to the DFG/D-motif of Mnk2 and by modifying the length of C6-carboxamide to reside in the HR2 region has yielded a series of compounds that inhibit Mnk2 at low nanomolar concentrations and exhibit good anti-leukemic activity in MV4-11 and MOLM-13 cells. In particular, compounds **7b**, **7c** and **7d** have similar high potency against Mnk2, which could be attributed to their bulkiness of C6-carboxamide substituents. Compound **7b** is the most potent derivative with K_i values of 106 nM and 18 nM against Mnk1 and Mnk2, respectively. In-house Mnk kinase assays also identified compound **7d** as a Mnk2-selective inhibitor that could be adopted as a powerful pharmacological tool to elucidate the Mnk-eIF4E-mediated tumorigenic mechanism. The molecular basis of activity and/or selectivity of compounds **7b** and **7d** against Mnks remain unknown due to the lack of an active Mnk1 and Mnk2 structure to facilitate such an investigation. In conclusion, this study suggests the potential utility of the thienopyrimidine derivatives as anti-leukemic agents.

4. Experimental section

4.1. Experimental procedures for computational-aided virtual screening

Openeye Scientific Software was utilized with Microsoft Window XP on a 2.66 GHz Intel Core2 processor system with 3.21 GB RAM for all virtual screening applications. Visual Interface to Drug design Application v4.0.3 (VIDA) [38] was used as the core graphical platform to access most of the Openeye modules; PICTO v4.0.3 [38], MAKE RECEPTOR v3.0.0 [39], Fast Rigid Exhaustive Docking (FRED) v3.0.0 [39] and vROCS v3.1.2 [40]. Other modules including Babel v3.3 [41], FILTER v2.1.1 [42] and OMEGA v2.4.6 [43] are driven by command line prompts.

4.1.1. 3D database preparation

Molecules including the three known Mnk inhibitors (*i.e.* CGP052088, CGP57380 and cercosporamide) and the previously in-house built database containing a total of 35 Mnk2 actives and inactives was prepared manually using the drawing tool PICTO and stored as a control database.

The ChemBridge database with over 572,000 2D purchasable compounds (March 2012), was obtained from the ZINC library. As the database contains only atom connectivity with no 3D structural information, it was converted to 1D notation using Babel. A data reduction tool, FILTER, was employed to eliminate compounds with molecular weight (MW) outside the range of 300–450 Da. This MW range is generally considered drug-like and thus was adopted in the filtering process. The filtered compounds comprising 387,000 compounds were saved as a screening database.

A maximum of 50 conformers for each molecule in these databases was generated by applying *–maxconfs* flag through OMEGA. Additionally, flags *–strictstereo* and *–canonOrder* were disabled to prevent the failure of conformer generation for molecules with specified stereo centers and to deactivate the automatic reordering of conformers to a canonical atom and bond order, respectively.

4.1.2. Database alignment against selected query molecules

Ligand-based approaches adopt the approach that compounds bearing structural similarity to a query molecule with known biological activity are likely to exert similar properties. The ROCS overlay method assigns a score based on a the concept of Gaussian volume overlap, which undertakes a rapid assessment of the centre-of-mass of the query and database molecules, overlays their principal components of inertia and hence maximizes the shared volume overlap [29]. ROCS was used to investigate such similarities between known Mnk2 inhibitors and the developed screening database. Both CGP57380 and cercosporamide were adopted as query molecules to account for the diversity of inhibitors involved. In order to utilize the most energetically favorable conformation, OMEGA was applied to generate one conformer for each query. The color force field dropdown in vROCS was adjusted to the ImplicitMillsDean option as it is the default setup that involves a pKa model assuming pH = 7. This automatically assigns appropriate physiologically relevant ionization states for each aligned molecule. Assessment of the conformers was computed by TanimotoCombo (shape and color (*i.e.* chemical features include anions, cations, hydrogen bond donors and acceptors, hydrophobes and rings) combination) as it has been found as the most useful metric in a number of other studies [44,45]. A total combo score of 2 indicates an identical match of both shape and color between a given molecule and a query. Each resulting alignment was analyzed by the inbuilt visualization tool, VIDA.

4.1.3. Database screening against Mnk2 protein kinase

The crystal structure of Mnk2 in complex with staurosporine (PDB ID code: 2HW7) was used for docking purposes, as the presence of a bound ligand in the crystal structure facilitates the docking program in defining the target active site. The docking experiments were performed using the OEDocking module with its complementary tools including MAKE RECEPTOR and FRED. Initially, the Mnk2 receptor binding site was defined by forming an enclosed box through molecular cavity detection in MAKE RECEPTOR. The active site shape was characterized by inner and outer contours of a shape potential. Every single heavy atom of a docked pose is required to fit within the shape of the outer contour and at least one heavy atom lies within the volume of the inner contour. Keeping the default settings, the defined receptor was ready for docking experiments [27]. The multi-conformer databases were respectively docked into the established receptor using the FRED

command-line prompt. The number of poses to be generated for each docked molecule was adjusted to 50 to allow a broad analysis of the docked poses in the active site. Each docking pose was evaluated by the default scoring function, Chemgauss4, and the screened candidates were ranked accordingly.

4.2. Synthesis of chemical compounds

Chemical reagents and solvents were purchased from commercial sources, and were used as received unless otherwise specified. All reactions except microwave-assisted synthesis were carried out with continuous magnetic stirring in ordinary glassware; microwave-assisted synthesis was performed in an Asynt DrySyn insert (10 mL) (Isleham, UK) using a CEM Discover SP and Explorer 48/72/96 microwave system (Matthews, NC, USA) controlled by Synergy™ software (Firmware version DSCA02.17). Reactions were monitored using thin layer chromatography (TLC), which was performed on Merck silica gel 60 F_{254} pre-coated aluminum plates (0.2 mm), and was visualized under UV light (254 nm). Flash column chromatography was carried out using either pre-packed silica gel cartridges KP-SIL (*ca.* 0.05 mm) on Biotage® Isolera™ Four automated flash chromatography or fritted solid loaders packed with Scharlau® silica gel (0.04–0.06 mm) on Biotage® FlashMaster Personal$^+$ flash chromatography. High resolution mass spectra were recorded using an AB SCIEX TripleTOF® 5600 mass spectrometer, and ionization of all samples was carried out using ESI. ^{1}H NMR and ^{13}C NMR spectra were obtained at 298 K using a Bruker AVANCE III HD spectrometer at 500.16 and 125.76 MHz, respectively, and were analyzed using a Bruker Topspin 3.2 program. ^{1}H and ^{13}C NMR spectra are referenced to ^{1}H signals of residual non deuterated solvents and ^{13}C signals of the deuterated solvents, respectively. ^{1}H NMR signals are reported with chemical shift values δ (ppm), multiplicity (s = singlet, d = doublet, t = triplet, q = quartet, dd = doublet of doublets, td = triplet of doublets, m = multiplet and br = broad), relative integral, coupling constants *J* (Hz) and assignments. The purity of compounds used for biological evaluations was determined to be greater than 95% using Shimadzu Prominence UltraFast Liquid Chromatography (UFLC) system (Kyoto, Japan) equipped with a CBM-20A communications bus module, a DGU-20A_{5R} degassing unit, an LC-20AD liquid chromatograph pump, an SIL-20A_{HT} auto-sampler, an SPD-M20A photo diode array detector, a CTO-20A column oven and a Phenomenex Kinetex 5 μM C18 100 Å 250 mm × 4.60 mm column. Method A (gradient 5%–95% MeOH containing 0.1% formic acid over 7 min at a flow rate of 1 mL/min, followed by 95% MeOH containing 0.1% formic acid over 13 min) and method B (gradient 5%–95% MeCN containing 0.1% formic acid over 7 min at a flow rate of 1 mL/min, followed by 95% MeCN containing 0.1% formic acid over 13 min) were used for analytic RP-HPLC. Melting points were determined using an open capillary on a Stuart SMP10 melting point apparatus, and are uncorrected.

The synthesis of analogs of hit **3**, *i.e.* 4-((4-fluorophenyl)amino)-5-methylthieno[2,3-*d*]pyrimidine-6-carboxylate derivatives is outlined in Scheme 1. Chlorination of methyl 5-methyl-4-oxo-3,4-dihydrothieno[2,3-*d*]pyrimidine-6-carboxylate **1** with thionyl chloride in the presence of *N*,*N*-dimethylformamide yielded methyl 4-chloro-5-methylthieno[2,3-*d*]pyrimidine-6-carboxylate **2** in a yield of 80%. Treatment of 4-fluoro-1-nitrobenzene **3a**, **3b** or **3c** with hydrogen gas in the presence of 10% Pd/C gave the corresponding amine **4a**, **4b** or **4c** in excellent yields (92–100%). The microwave-assisted coupling of amine **4a**, **4b** or **4c** to chloride **2** was carried out in 1,4-dioxane in the presence of *p*-toluenesulfonic acid to give the corresponding methyl 4-((4-fluorophenyl)amino)-5-methylthieno[2,3-*d*]pyrimidine-6-carboxylate **5a**, **5b** or **5c**. The subsequent saponification of ester **5a**, **5b** or **5c** was accomplished using either sodium hydroxide or lithium hydroxide in a mixture of tetrahydrofuran/methanol/water to give the corresponding carboxylic acid **6a**, **6b** or **6c** in good to excellent yields (67–91%). Amidation of carboxylic acid **6c** with appropriate amines resulted in amides **7a-e**.

4.2.1. Methyl 4-chloro-5-methylthieno[2,3-d]pyrimidine-6-carboxylate (**2**)

To a solution of methyl 5-methyl-4-oxo-3,4-dihydrothieno[2,3-*d*]pyrimidine-6-carboxylate (**1**, 2.00 g, 8.92 mmol) in $SOCl_2$ (20.0 mL, 276 mmol) was added DMF (400 μL, 5.19 mmol). The reaction mixture was heated at reflux under N_2 for 2 h and concentrated under reduced pressure. The residue was purified by Biotage® FlashMaster Personal$^+$ flash chromatography (silica gel, DCM ramping to DCM:EtOAc = 99:1) to give **2** as a white solid (1.73 g, 80%). $\boldsymbol{R_F}$ (DCM:EtOAc = 98:2) 0.57. **m.p.** 141–142 °C. **^{1}H NMR** ($CDCl_3$) δ 2.97 (s, 3H, thiophene-CH_3), 3.91 (s, 3H, $COOCH_3$), 8.79 (s, 1H, pyrimidine-H). **^{13}C NMR** ($CDCl_3$) δ 15.8, 52.8, 127.9, 128.8, 139.2, 154.2, 157.3, 162.4, 169.1. **HRMS** (ESI) *m/z* 243.0032 [M(^{35}Cl)+H]$^+$, 245.0000 [M(^{37}Cl)+H]$^+$; calcd. for $C_9H_8ClN_2O_2S^+$ 242.9990 [M(^{35}Cl)+H]$^+$, 244.9960 [M(^{37}Cl)+H]$^+$.

4.2.2. 4-Fluoroaniline (**4a**)

To a solution of 4-fluoro-1-nitrobenzene (**3a**, 212 μL, 2.00 mmol) in MeOH (10 mL) was added 10% Pd/C (21 mg, 0.020 mmol). The reaction mixture was stirred and bubbled with H_2 at room temperature for 3 h. The solids were filtered off and washed with DCM (25 mL). The filtrate and DCM washing were combined and concentrated under reduced pressure to give **4a** as a clear yellow oil (222 mg, 100%). **HRMS** (ESI) *m/z* 112.0541 [M+H]$^+$; calcd. for $C_6H_7FN^+$ 112.0558 [M+H]$^+$.

4.2.3. 4-Fluoro-2-methylaniline (**4b**)

To a solution of 4-fluoro-2-methyl-1-nitrobenzene (**3b**, 243 μL, 2.00 mmol) in MeOH (10 mL) was added 10% Pd/C (21 mg, 0.020 mmol). The reaction mixture was stirred and bubbled with H_2 at room temperature for 2 h. The solids were filtered off and washed with DCM (25 mL). The filtrate and DCM washing were combined and concentrated under reduced pressure. The residue was purified by flash column chromatography (silica gel, P.E. ramping to PE:EtOAc = 4:1) to give **4b** as a pink oil (250 mg, 100%). $\boldsymbol{R_F}$ (EtOAc:PE = 1:4) 0.18. **^{1}H NMR** ($CDCl_3$) δ 2.03 (s, 3H, CH_3), 4.65 (s, 2H, NH_2), 6.56 (dd, 1H, *J* 5.0 & 8.5, benzene-H), 6.70 (td, 1H, *J* 3.0 & 9.0, benzene-H), 6.77 (dd, 1H, *J* 3.0 & 9.5, benzene-H). **HRMS** (ESI) *m/z* 126.0778 [M+H]$^+$; calcd. for $C_7H_9FN^+$ 126.0714 [M+H]$^+$.

4.2.4. 4-Fluoro-2-isopropoxyaniline (**4c**)

To a solution of 4-fluoro-2-isopropxy-1-nitrobenzene (**3c**, 199 mg, 0.999 mmol) in anhydrous EtOH (10 mL) was added 10% Pd/C (11 mg, 0.010 mmol). The reaction mixture was stirred and bubbled with H_2 at room temperature for 2 h. The solids were filtered off and washed with DCM (25 mL). The filtrate and DCM washing were combined and concentrated under reduced pressure. The residue was purified by Biotage® Isolera™ Four automated flash chromatography (Biotage® SNAP cartridge KP-Sil 10 g, hexane ramping to EtOAc:hexane = 1:4) to give **4c** as a colorless oil (155 mg, 92%). $\boldsymbol{R_F}$ (PE:EtOAc = 9:1) 0.40. **^{1}H NMR** ($CDCl_3$) δ 1.35 (d, 6H, *J* 6.0, 2 × CH_3), 3.72 (s, 2H, NH_2), 4.44–4.52 (m, 1H, O*CH*(CH_3)$_2$), 6.49 (td, 1H, *J* 8.5 & 2.5, benzene-H), 6.57 (dd, 1H, *J* 10.5 & 3.0, benzene-H), 6.63 (dd, 1H, *J* 8.5 & 5.5, benzene-H). **^{13}C NMR** ($CDCl_3$) δ 22.1, 71.0, 101.5 (d, $J_{C\text{-}F}$ 25.9), 106.5 (d, $J_{C\text{-}F}$ 22.0), 115.1 (d, $J_{C\text{-}F}$ 9.1), 132.9 (d, $J_{C\text{-}F}$ 2.5), 146.0 (d, $J_{C\text{-}F}$ 9.6), 156.3 (d, $J_{C\text{-}F}$ 234.3) (one carbon signal overlapping or obscured). **HRMS** (ESI) *m/z* 170.1144 [M+H]$^+$; calcd. for $C_9H_{13}FNO^+$ 170.0976 [M+H]$^+$. The spectroscopic data were in agreement with those in the literature [46].

*4.2.5. Methyl 4-((4-fluorophenyl)amino)-5-methylthieno[2,3-d] pyrimidine-6-carboxylate (**5a**)*

To a solution of **4a** (222 mg, 2.00 mmol) in 1,4-dioxane (3.5 mL) were added **2** (485 mg, 2.00 mmol) and TsOH·H_2O (77 mg, 0.40 mmol). The reaction mixture was heated at 150 °C under microwave irradiation for 0.5 h and concentrated under reduced pressure. The residue was purified by flash column chromatography (silica gel, P.E. ramping to PE:EtOAc = 7:3) and recrystallized (hexane:acetone = 1:5) to give **5a** as greenish needles (114 mg, 18%). R_F (EtOAc:PE = 1:1) 0.61. **m.p.** 191–193 °C. ^{1}**H NMR** (DMSO-d_6) δ 3.13 (s, 3H, CH_3), 3.93 (s, 3H, OCH_3), 7.14 (t, 2H, *J* 8.5, benzene-H), 7.58–7.62 (m, 3H, benzene-H & NH), 8.54 (s, 1H, pyrimidine-H). ^{13}**C NMR** (DMSO-d_6) δ 16.0, 52.6, 116.1 (d, $J_{C\text{-}F}$ 22.6), 117.5, 124.2, 124.9 (d, $J_{C\text{-}F}$ 13.1), 133.2 (d, $J_{C\text{-}F}$ 2.9), 137.4, 154.5, 157.5, 159.4, 161.3, 163.0 (two carbon signals overlapping or obscured). **HRMS** (ESI) *m/z* 318.0694 $[M+H]^+$; calcd. for $C_{15}H_{13}FN_3O_2S^+$ 318.0708 $[M+H]^+$. **Anal. RP-HPLC** Method A: t_R 11.38 min, purity >95%; Method B: t_R 12.48 min, purity >95%.

*4.2.6. Methyl 4-((4-fluoro-2-methylphenyl)amino)-5-methylthieno [2,3-d]pyrimidine-6-carboxylate (**5b**)*

To a solution of **4b** (250 mg, 2.00 mmol) in 1,4-dioxane (3.5 mL) were added **2** (485 mg, 2.00 mmol) and TsOH·H_2O (76 mg, 0.40 mmol). The reaction mixture was heated at 150 °C under microwave irradiation for 0.5 h and concentrated under reduced pressure. The residue was purified by flash column chromatography (silica gel, P.E. ramping to PE:EtOAc = 4:1) and recrystallized (hexane:acetone = 1:5) to give **5b** as greenish needles (209 mg, 32%). R_F (EtOAc:PE = 1:1) 0.54. **m.p.** 243–245 °C. ^{1}**H NMR** ($CDCl_3$) δ 2.31 (s, 3H, CH_3), 3.13 (s, 3H, CH_3), 3.94 (s, 3H, OCH_3), 7.00–7.04 (m, 2H, benzene-H), 7.34 (s, 1H, NH), 7.61 (dd, 1H, *J* 5.0 & 8.0, benzene-H), 8.52 (s, 1H, pyrimidine-H). ^{13}**C NMR** ($CDCl_3$) δ 16.1, 18.7, 52.6, 113.8 (d, $J_{C\text{-}F}$ 22.4), 117.5, 117.7 (d, $J_{C\text{-}F}$ 22.5), 124.1, 127.8 (d, $J_{C\text{-}F}$ 22.5), 131.4 (d, $J_{C\text{-}F}$ 2.8), 135.4 (d, $J_{C\text{-}F}$ 8.3), 137.5, 154.7, 158.1, 160.1, 162.1, 163.0. **HRMS** (ESI) *m/z* 332.1376; calcd. for $C_{16}H_{15}FN_3O_2S^+$ 332.0864 $[M+H]^+$. **Anal. RP-HPLC** Method A: t_R 11.00 min, purity >99%; Method B: t_R 10.04 min, purity >98%.

*4.2.7. Methyl 4-((4-fluoro-2-isopropoxyphenyl)amino)-5-methylthieno[2,3-d]pyrimidine-6-carboxylate (**5c**)*

To a solution of **4c** (153 mg, 0.904 mmol) in 1,4-dioxane (3 mL) were added **2** (219 mg, 0.902 mmol) and TsOH·H_2O (35 mg, 0.18 mmol). The reaction mixture was heated at 150 °C under microwave irradiation for 0.5 h and concentrated under reduced pressure. The residue was dissolved in DCM (25 mL) and washed with H_2O (4 × 25 mL). The organic layer was dried over Na_2SO_4 and concentrated under reduced pressure. The residue was purified by Biotage® FlashMaster Personal$^+$ flash chromatography (silica gel, DCM ramping to DCM:EtOAc = 97:3) to give **5c** as a white solid (268 mg, 79%). R_F (DCM:EtOAc = 98:2) 0.33. **m.p.** 182–183 °C. ^{1}**H NMR** ($CDCl_3$) δ 1.43 (d, 6H, *J* 6.0, $OCH(CH_3)_2$), 3.12 (s, 3H, thiophene-CH_3), 3.91 (s, 3H, $COOCH_3$), 4.61–4.69 (m, 1H, $OCH(CH_3)_2$), 6.67 (dd, 1H, *J* 10.0 & 2.5, benzene-H), 6.71 (td, 1H, *J* 9.0 & 2.5, benzene-H), 8.44 (s, 1H, NH), 8.59 (s, 1H, pyrimidine-H), 8.75 (dd, 1H, *J* 9.0 & 6.5, benzene-H). ^{13}**C NMR** ($CDCl_3$) δ 15.8, 22.2, 52.5, 71.8, 100.4 (d, $J_{C\text{-}F}$ 26.9), 106.7 (d, $J_{C\text{-}F}$ 21.6), 118.0, 121.7 (d, $J_{C\text{-}F}$ 9.0), 123.4, 124.8 (d, $J_{C\text{-}F}$ 3.0), 137.6, 147.6 (d, $J_{C\text{-}F}$ 9.8), 154.9, 156.3, 159.1 (d, $J_{C\text{-}F}$ 241.5), 163.2, 166.2 (one carbon signal overlapping or obscured). **HRMS** (ESI) *m/z* 376.1207 $[M+H]^+$; calcd. for $C_{18}H_{19}FN_3O_3S^+$ 376.1126 $[M+H]^+$. **Anal. RP-HPLC** Method A: t_R 13.98 min, purity >98%; Method B: t_R 13.19 min, purity >97%.

*4.2.8. 4-((4-Fluorophenyl)amino)-5-methylthieno[2,3-d] pyrimidine-6-carboxylic acid (**6a**)*

To a solution of **5a** (89 mg, 0.28 mmol) in 1 M aqueous NaOH solution (1 mL, 1 mmol) were added MeOH (5 mL) and THF (5 mL). The reaction mixture was stirred at 70 °C for 4 h and quenched with 1 M aqueous HCl solution (1 mL, 1 mmol). The organic solvents were removed under reduced pressure, and the precipitate was filtered off, washed with H_2O (3 × 10 mL) and dried *in vacuo* to give **6a** as a white solid (74 mg, 87%). R_F (EtOAc:PE = 1:1) 0.05. **m.p.** 293–295 °C. ^{1}**H NMR** (DMSO-d_6) δ 3.03 (s, 3H, CH_3), 7.22 (t, 2H, *J* 8.5, benzene-H), 7.62 (dd, 2H, *J* 3.5 & 8.5, benzene-H), 8.45 (s, 1H, pyridine-H), 8.63 (s, 1H, NH). ^{13}**C NMR** (DMSO-d_6) δ 15.5, 115.2 (d, $J_{C\text{-}F}$ 22.5), 117.8, 123.6, 125.8 (d, $J_{C\text{-}F}$ 7.5), 134.9, 138.8, 155.0 (d, $J_{C\text{-}F}$ 15.0), 157.3, 158.1, 160.1, 164.0, 166.9 (one carbon signal overlapping or obscured). **HRMS** (ESI) *m/z* 304.0660 $[M+H]^+$; calcd. for $C_{14}H_{11}FN_3O_2S^+$ 304.0551 $[M+H]^+$. **Anal. RP-HPLC** Method A: t_R 10.38 min, purity >97%; Method B: t_R 8.62 min, purity >99%.

*4.2.9. 4-((4-Fluoro-2-methylphenyl)amino)-5-methylthieno[2,3-d] pyrimidine-6-carboxylic acid (**6b**)*

To a solution of **5b** (164 mg, 0.50 mmol) in 1 M aqueous NaOH solution (1 mL, 1 mmol) were added MeOH (5 mL) and THF (5 mL). The reaction mixture was stirred at 70 °C for 4 h and quenched with 1 M aqueous HCl solution (1 mL, 1 mmol). The organic solvents were removed under reduced pressure, and the precipitate was filtered off, washed with water (3 × 10 mL) and dried *in vacuo* to give **6b** as a white solid (145 mg, 91%). R_F (EtOAc:PE = 1:1) 0.03. **m.p.** 294–296 °C. ^{1}**H NMR** (DMSO-d_6) δ 2.18 (s, 3H, CH_3), 3.03 (s, 3H, CH_3), 7.07 (dt, 1H, *J* 3.0 & 8.5, benzene-H), 7.17 (dd, 1H, *J* 3.0 & 9.5, benzene-H), 7.40 (dd, 1H, *J* 5.5 & 8.5, benzene-H), 8.33 (s, 1H, pyrimidine-H), 8.48 (s, 1H, NH). ^{13}**C NMR** (DMSO-d_6) δ 15.7, 18.2, 112.8 (d, $J_{C\text{-}F}$ 21.9), 116.7 (d, $J_{C\text{-}F}$ 22.1), 123.0, 129.4 (d, $J_{C\text{-}F}$ 8.6), 133.4 (d, $J_{C\text{-}F}$ 2.5), 137.8 (d, $J_{C\text{-}F}$ 8.3), 139.0, 155.3, 157.9, 159.4, 161.3, 164.0, 166.8. **HRMS** (ESI) *m/z* 318.0830 $[M+H]^+$; calcd. for $C_{15}H_{13}FN_3O_2S^+$ 318.0708 $[M+H]^+$. **Anal. RP-HPLC** Method A: t_R 10.28 min, purity >97%; Method B: t_R 8.59 min, purity >99%.

*4.2.10. 4-((4-Fluoro-2-isopropoxyphenyl)amino)-5-methylthieno [2,3-d]pyrimidine-6-carboxylic acid (**6c**)*

To a solution of **5c** (200 mg, 0.533 mmol) in a mixture of THF/MeOH/H_2O (1:1:1, 60 mL) was added LiOH (382 mg, 16.0 mmol). The reaction mixture was stirred at room temperature overnight and washed with DCM (20 mL). The aqueous layer was heated at 50 °C for 10 min and acidified to pH 3 with 2 M HCl. The precipitate was filtered, washed with H_2O (3 × 25 mL) and dried under reduced pressure to give **6c** as a white solid (128 mg, 67%). R_F (DCM:MeOH = 9:1) 0.28. **m.p.** > 300 °C. ^{1}**H NMR** (DMSO-d_6) δ 1.32 (d, 6H, *J* 6.0, $OCH(CH_3)_2$), 3.07 (s, 3H, thiophene-CH_3), 4.75–4.80 (m, 1H, $OCH(CH_3)_2$), 6.80 (td, 1H, *J* 8.5 & 2.5, benzene-H), 7.07 (dd, 1H, *J* 11.0 & 2.5, benzene-H), 8.47 (s, 1H, NH), 8.54 (s, 1H, pyrimidine-H), 8.56 (dd, 1H, *J* 9.0 & 6.5, benzene-H) (one carboxylic acid proton signal not observed). ^{13}**C NMR** (DMSO-d_6) δ 15.3, 21.7, 71.5, 101.1 (d, $J_{C\text{-}F}$ 26.8), 106.1 (d, $J_{C\text{-}F}$ 21.6), 117.8, 121.9 (d, $J_{C\text{-}F}$ 9.4), 123.9, 125.0 (d, $J_{C\text{-}F}$ 2.6), 137.5, 148.3 (d, $J_{C\text{-}F}$ 10.6), 155.1, 156.1, 158.6 (d, $J_{C\text{-}F}$ 239.0), 163.9, 166.3 (one carbon signal overlapping or obscured). **HRMS** (ESI) *m/z* 362.1500 $[M+H]^+$; calcd. for $C_{17}H_{17}FN_3O_3S^+$ 362.0969 $[M+H]^+$. **Anal. RP-HPLC** Method A: t_R 16.95 min, purity >97%; Method B: t_R 12.48 min, purity >97%.

*4.2.11. 4-((4-Fluoro-2-isopropoxyphenyl)amino)-5-methylthieno [2,3-d]pyrimidine-6-carboxamide (**7a**)*

To a solution of **6c** (160 mg, 0.442 mmol) in DMF (3 mL) were added DIPEA (160 μL, 0.919 mmol) and HATU (190 mg, 0.500 mmol). The reaction mixture was stirred on an ice bath for 30 min. NH_3 (7 M in MeOH, 220 μL, 1.54 mmol) was added, and the reaction mixture was stirred at room temperature overnight and concentrated under reduced pressure. The residue was purified by Biotage® FlashMaster Personal$^+$ flash chromatography (silica gel,

DCM ramping to DCM:EtOAc = 4:1) to give **7a** as a white solid (138 mg, 86%). R_F (MeOH:EtOAc = 1:5) 0.43. **m.p.** 159–160 °C. **^{1}H NMR** (DMSO-d_6) δ 1.33 (d, 6H, *J* 6.0, OCH(CH_3)$_2$), 2.95 (s, 3H, thiophene-CH_3), 4.78–4.83 (m, 1H, OC*H*(CH_3)$_2$), 6.83 (td, 1H, *J* 8.5 & 2.5, benzene-H), 7.10 (dd, 1H, *J* 11.0 & 3.0, benzene-H), 7.83 (br d, 2H, *J* 56.0, NH_2), 8.43 (s, 1H, pyrimidine–NH–benzene), 8.54 (s, 1H, pyrimidine-H), 8.58 (dd, 1H, *J* 9.0 & 6.5, benzene-H).**^{13}C NMR** (DMSO-d_6) δ 15.8, 22.7, 71.4, 101.1 (d, $J_{C\text{-}F}$ 26.8), 106.0 (d, $J_{C\text{-}F}$ 21.7), 117.3, 121.8 (d, $J_{C\text{-}F}$ 9.3), 125.1 (d, $J_{C\text{-}F}$ 2.7), 128.6, 131.1, 148.2 (d, $J_{C\text{-}F}$ 10.2), 154.3, 155.7, 158.5 (d, $J_{C\text{-}F}$ 238.9), 163.9, 165.3 (one carbon signal overlapping or obscured). **HRMS** (ESI) *m/z* 361.1135 $[M+H]^+$; calcd. for $C_{17}H_{18}FN_4O_2S^+$ 361.1129 $[M+H]^+$. **Anal. RP-HPLC** Method A: t_R 15.88 min, purity >98%; Method B: t_R 11.63 min, purity >95%.

4.2.12. 4-((4-Fluoro-2-isopropoxyphenyl)amino)-N,5-dimethylthieno[2,3-d]pyrimidine-6-carboxamide (**7b**)

To a solution of **6c** (55 mg, 0.15 mmol) in DMF (3 mL) were added DIPEA (40 μL, 0.23 mmol) and HATU (80 mg, 0.21 mmol). The reaction mixture was stirred on an ice bath for 30 min. Methylamine hydrochloride (80 mg, 1.2 mmol) was added, and the reaction mixture was stirred at room temperature overnight, and concentrated under reduced pressure. The residue was purified by Biotage® FlashMaster Personal$^+$ flash chromatography (silica gel, DCM ramping to DCM:EtOAc = 4:1) to give **7b** as a white solid (35 mg, 63%). R_F (DCM:EtOAc = 4:1) 0.44. **m.p.** 223–224 °C. **^{1}H NMR** (DMSO-d_6) δ 1.33 (d, 6H, *J* 6.0, OCH(CH_3)$_2$), 2.79 (d, 3H, *J* 4.5, NHCH_3), 2.92 (s, 3H, thiophene-CH_3), 4.77–4.83 (m, 1H, OC*H*(CH_3)$_2$), 6.83 (td, 1H, *J* 11.5 & 8.5, benzene-H), 7.10 (dd, 1H, *J* 10.5 & 2.5, benzene-H), 8.40 (q, 1H, *J* 4.5, N*H*CH_3), 8.42 (s, 1H, pyrimidine–NH–benzene), 8.54 (s, 1H, pyrimidine-H), 8.58 (dd, 1H, *J* 9.0 & 6.5, benzene-H). **^{13}C NMR** (DMSO-d_6) δ 15.8, 21.7, 26.5, 71.4, 101.1 (d, $J_{C\text{-}F}$ 3.2), 106.0 (d, $J_{C\text{-}F}$ 21.7), 117.2, 122.8 (d, $J_{C\text{-}F}$ 9.2), 125.1 (d, $J_{C\text{-}F}$ 2.7), 128.4, 130.6, 148.2 (d, $J_{C\text{-}F}$ 10.5), 154.3, 155.7, 158.5 (d, $J_{C\text{-}F}$ 238.7), 162.6, 165.2 (one carbon signal overlapping or obscured). **HRMS** (ESI) *m/z* 375.1525 $[M+H]^+$; calcd. for $C_{18}H_{20}FN_4O_2S^+$ 375.1286 $[M+H]^+$. **Anal. RP-HPLC** Method A: t_R 16.06 min, purity >95%; Method B: t_R 12.00 min, purity >96%.

4.2.13. N-Ethyl-4-((4-fluoro-2-isopropoxyphenyl)amino)-5-methylthieno[2,3-d]pyrimidine-6-carboxamide (**7c**)

To a solution of **6c** (50 mg, 0.14 mmol) in DMF (3 mL) were added DIPEA (40 μL, 0.23 mmol) and HATU (80 mg, 0.21 mmol). The reaction mixture was stirred on an ice bath for 30 min. Ethylamine (2.0 M in THF, 1.0 mL, 2.0 mmol) was added, and the reaction mixture was stirred at room temperature overnight and concentrated under reduced pressure. The residue was dissolved in DCM (20 mL), washed with saturated $NaHCO_3$ (3 × 20 mL), 10% citric acid (3 × 20 mL), H_2O (3 × 20 mL) and brine (3 × 20 mL), and concentrated under reduced pressure. The residue was purified by Biotage® FlashMaster Personal$^+$ flash chromatography (silica gel, DCM ramping to DCM:EtOAc = 4:1) to give **7c** as a white solid (18 mg, 34%). R_F (DCM:EtOAc = 4:1) 0.29. **m.p.** 205–206 °C. **^{1}H NMR** ($CDCl_3$) δ 1.28 (t, 3H, *J* 7.0, NHCH_2CH_3), 1.42 (d, 6H, *J* 6.0, OCH(CH_3)$_2$), 3.05 (s, 3H, thiophene-CH_3), 3.46–3.53 (m, 2H, NHCH_2CH$_3$), 4.63–4.69 (m, 1H, OC*H*(CH_3)$_2$), 6.02 (br s, 1H, N*H*CH_2CH_3), 6.68 (dd, 1H, *J* 10.5 & 2.5, benzene-H), 6.72 (td, 1H, *J* 9.0 & 6.0, benzene-H), 8.42 (s, 1H, pyrimidine–NH–benzene), 8.58 (s, 1H, pyrimidine-H), 8.77 (dd, 1H, *J* 9.0 & 6.5, benzene-H). **^{13}C NMR** ($CDCl_3$) δ 15.0, 16.1, 22.2, 29.8, 35.4, 71.8, 100.4 (d, $J_{C\text{-}F}$ 27.5), 106.7 (d, $J_{C\text{-}F}$ 21.3), 118.3, 121.5 (d, $J_{C\text{-}F}$ 8.8), 125.0 (d, $J_{C\text{-}F}$ 3.8), 127.1, 132.8, 147.6 (d, $J_{C\text{-}F}$ 10.0), 154.5, 156.2, 159.0 (d, $J_{C\text{-}F}$ 241.3), 162.8 (one carbon signal overlapping or obscured). **HRMS** (ESI) *m/z* 389.1443 $[M+H]^+$; calcd. for $C_{19}H_{22}FN_4O_2S^+$ 389.1442 $[M+H]^+$. **Anal. RP-HPLC** Method A: t_R 16.20 min, purity >97%; Method B: t_R 12.29 min, purity >97%.

4.2.14. 4-((4-Fluoro-2-isopropoxyphenyl)amino)-N-(2-methoxyethyl)-5-methylthieno[2,3-d]pyrimidine-6-carboxamide (**7d**)

To a solution of **6c** (200 mg, 0.553 mmol) in DMF (3 mL) were added DIPEA (193 μL, 1.11 mmol) and HATU (316 mg, 0.830 mmol). The reaction mixture was stirred on an ice bath for 30 min. 2-Methoxypropylamine (54.0 μL, 0.609 mmol) was added, and the reaction mixture was stirred at room temperature overnight and concentrated under reduced pressure. The residue was dissolved in DCM (20 mL), washed with saturated $NaHCO_3$ (3 × 20 mL), 10% citric acid (3 × 20 mL), H_2O (3 × 20 mL) and brine (3 × 20 mL), and concentrated under reduced pressure. The residue was purified by Biotage® FlashMaster Personal$^+$ flash chromatography (silica gel, DCM ramping to DCM:EtOAc = 4:1) to give **7d** as a white solid (118 mg, 51%). R_F (DCM:EtOAc = 7:3) 0.54. **m.p.** 186–187 °C. **^{1}H NMR** ($CDCl_3$) δ 1.43 (d, 6H, *J* 6.0, OCH(CH_3)$_2$), 3.06 (s, 3H, thiophene-CH_3), 3.41 (s, 3H, OCH_3), 3.56–3.60 (m, 2H, CH_2CH_2O), 3.63–3.67 (m, 2H, CH_2CH_2O), 4.64–4.69 (m, 1H, OC*H*(CH_3)$_2$), 6.34 (br s, 1H, CONH), 6.69 (dd, 1H, *J* 10.0 & 3.0, benzene-H), 6.73 (td, 1H, *J* 8.5 & 2.5, benzene-H), 8.47 (br s, 1H, pyrimidine–NH–benzene), 8.61 (s, 1H, pyrimidine-H), 8.77 (dd, 1H, *J* 9.0 & 6.5, benzene-H). **^{13}C NMR** ($CDCl_3$) δ 16.1, 22.2, 40.1, 59.1, 70.3, 71.9, 100.5 (d, $J_{C\text{-}F}$ 27.0), 106.8 (d, $J_{C\text{-}F}$ 21.6), 118.3, 121.7 (d, $J_{C\text{-}F}$ 9.0), 124.9, 127.3, 132.9, 147.7 (d, $J_{C\text{-}F}$ 9.5), 154.2, 156.2, 159.1 (d, $J_{C\text{-}F}$ 241.5), 162.9 (two carbon signals overlapping or obscured). **HRMS** (ESI) *m/z* 419.1394 $[M+H]^+$; calcd. for $C_{20}H_{24}FN_4O_3S^+$ 419.1548 $[M+H]^+$. **Anal. RP-HPLC** Method A: t_R 16.01 min, purity >96%; Method B: t_R 11.98 min, purity >96%.

4.2.15. 4-((4-Fluoro-2-isopropoxyphenyl)amino)-N-(3-methoxypropyl)-5-methylthieno[2,3-d]pyrimidine-6-carboxamide (**7e**)

To a solution of **6c** (65 mg, 0.18 mmol) in DMF (3 mL) were added DIPEA (58 μL, 0.33 mmol) and HATU (75 mg, 0.20 mmol). The reaction mixture was stirred on an ice bath for 30 min. 3-Methoxypropylamine (37 μL, 0.36 mmol) was added, and the reaction mixture was stirred at room temperature overnight and concentrated under reduced pressure. The residue was dissolved in DCM (20 mL), washed with saturated $NaHCO_3$ (3 × 20 mL), 10% citric acid (3 × 20 mL), H_2O (3 × 20 mL) and brine (3 × 20 mL), and concentrated under reduced pressure. The residue was purified by Biotage® FlashMaster Personal$^+$ flash chromatography (silica gel, DCM ramping to DCM:EtOAc = 1:1) to give **7e** as a white solid (37 mg, 48%). R_F (DCM:EtOAc = 7:3) 0.32. **m.p.** 170–171 °C. **^{1}H NMR** ($CDCl_3$) δ 1.43 (d, 6H, *J* 6.0, OCH(CH_3)$_2$), 1.88–1.93 (m, 2H, $CH_2CH_2CH_2$), 3.08 (s, 3H, thiophene-CH_3), 3.41 (s, 3H, OCH_3), 3.56–3.60 (m, 4H, CH_2CH$_2$CH_2), 4.64–4.70 (m, 1H, OC*H*(CH_3)$_2$), 6.70 (dd, 1H, *J* 10.0 & 2.5, benzene-H), 6.74 (td, 1H, *J* 8.5 & 2.5, benzene-H), 6.98 (br s, 1H, CONH), 8.59 (s, 1H, pyrimidine–NH–benzene), 8.61 (s, 1H, pyrimidine-H), 8.75 (dd, 1H, *J* 9.0 & 6.0, benzene-H). **^{13}C NMR** ($CDCl_3$) δ 16.0, 22.2, 28.7, 39.8, 59.2, 71.9, 72.7, 100.5 (d, $J_{C\text{-}F}$ 27.0), 106.8 (d, $J_{C\text{-}F}$ 21.6), 118.4, 121.7 (d, $J_{C\text{-}F}$ 9.0), 124.9, 127.9, 132.6, 147.7 (d, $J_{C\text{-}F}$ 9.7), 154.0, 156.2, 159.1 (d, $J_{C\text{-}F}$ 254.2), 162.5 (two carbon signals overlapping or obscured). **HRMS** (ESI) *m/z* 433.1538 $[M+H]^+$; calcd. for $C_{21}H_{26}FN_4O_3S^+$ 433.1704 $[M+H]^+$. **Anal. RP-HPLC** Method A: t_R 16.25 min, purity >98%; Method B: t_R 12.25 min, purity >98%.

4.3. Chemical and proteins

The Mnk inhibitor N^3-(4-fluorophenyl)-1*H*-pyrazolo-[3,4-*d*]pyrimidine-3,4-diamine (CGP57380) and cercosporamide were purchased from Sigma Aldrich and BioAustralis, respectively, and used as standard references or controls. All the compounds used were dissolved in dimethylsulfoxide (DMSO) at a stock concentration of 10 mM, and stored at −20 °C in small aliquots. eIF4E-derived

peptides: TAMRA-DTATKSGSTTKNR, TAMRA-DTATKSG(phospho) STTKNR and DTATKSGSTTKNR, were custom synthesized from Mimotopes Pty. Ltd. (Melbourne, Australia). Proteins Mnk1a and Mnk2a were purchased from Life Technologies and Merck Millipore, respectively.

4.4. Cell culture

Both MOLM-13 and MV4-11 cells were kindly provided by Prof. Richard D'Andrea (University of South Australia, Australia) and were maintained in Roswell Park Memorial Institute (RPMI)-1640 with 10% fetal bovine serum (FBS).

4.5. Kinase activity

The Millipore KinaseProfiler™ services were used to measure inhibition of Mnk2 (applied on virtual screening hits only), CDK2/cyclin A and CDK9/cyclin T1 with a radiometric assay format. The ATP concentrations were adjusted to K_m(app) for each kinase and half-maximal inhibition (IC_{50}) values were calculated from 10-point dose–response curves and apparent inhibition constants (K_i) were calculated from the IC_{50} values and appropriate K_m (ATP) values for the kinases in question using the Cheng-Prusoff equation [54].

4.5.1. IMAP™ TR-FRET progressive binding system

The inhibitors (1 and 10 μM in 0.5% DMSO) were added to the kinase reaction containing 1 × IMAP reaction buffer with Tween-20, dithiothreitol (DTT), dH_2O, TAMRA-labeled eIF4E peptide substrate and Mnk kinases (a total assay volume 20 μl) and incubated for 10 min. The reactions were sequentially started by adding ATP. The kinase reaction was run for 90 min at 30 °C and stopped with 60 μl progressive binding solution (30% binding buffer A, 70% binding buffer B, progressive binding reagent (1:600), Tb-donor (1:400)), followed by incubation in the dark for 5 h. After the incubation, the plate was read in EnVision multi-label plate reader (PerkinElmer, Beaconsfield, Buckinghamshire, UK). Excitation wavelength was set to 330 nm (Tb excitation) and emission was measured at 545 nm (Tb emission) and 572 nm (TR-FRET emission). Emission was measured in a time-resolved manner with a delay of 200 μsec. Positive and negative controls were also included with and without Mnk kinases, respectively, in 0.5% DMSO.

4.5.2. ADP-Glo™ kinase assay

Serial dilution of the inhibitor with a dilution factor of 1:3 was carried out for 8 different concentrations, ranging from 10 μM to 4.5 nM, in 0.5% DMSO. The inhibitors were added to the kinase reaction containing 1 × kinase reaction buffer, 1 mM bovine serum albumin (BSA), dH_2O, eIF4E peptide substrate and Mnk kinases (a total assay volume of 15 μl) and incubated for 10 min. The reactions were sequentially started by adding ATP. The kinase reaction was run for 45 min at 30 °C and stopped with 15 μl ADP Glo reagent, followed by incubation in the dark for 40 min. After the incubation, 30 μl of detection reagent was added and further incubated for 40 min before read in EnVision multi-label plate reader (PerkinElmer). Positive and negative controls were also included with and without Mnk kinases, respectively, in 0.5% DMSO.

4.6. Cell viability assay

Resazurin (Sigma Aldrich) assays were performed in MOLM-13 and MV4-11 cells as previously reported [16]. Compound concentrations required to inhibit 50% of cell growth (GI_{50}) were calculated using non-linear regression analysis.

Acknowledgment

This work is supported by funding from Australia Government National Health and Medical Research Council (project grant 1050825 to S.W.), and South Australian Health and Medical Research Institute, Beat Cancer Project Principal Cancer Research Fellowship, to S.W. We thank Dr Frankie Lam for assistance in assay development. We are grateful to Professor Richard D'Andrea (University of South Australia) for the generous supply of the AML cell lines.

Appendix A. Supplementary data

Supplementary data related to this article can be found at http://dx.doi.org/10.1016/j.ejmech.2015.09.008.

References

[1] M.J. Clemens, U.A. Bommer, Translational control: the cancer connection, Int. J. Biochem. Cell Biol. 31 (1999) 1–23.
[2] Y. Mamane, E. Petroulakis, L. Rong, K. Yoshida, L.W. Ler, N. Sonenberg, eIF4E-from translation to transformation, Oncogene 23 (2004) 3172–3179.
[3] S. Diab, M. Kumarasiri, M. Yu, T. Teo, C. Proud, R. Milne, S. Wang, MAP kinase-interacting kinases-emerging targets against cancer, Chem. Biol. 21 (2014) 441–452.
[4] R.E. Rhoads, eIF4E: new family members, new binding partners, new roles, J. Biol. Chem. 284 (2009) 16711–16715.
[5] J. Hou, F. Lam, C. Proud, S. Wang, Targeting Mnks for cancer therapy, Oncotarget 3 (2012) 118–131.
[6] R. Duncan, S.C. Milburn, J.W. Hershey, Regulated phosphorylation and low abundance of HeLa cell initiation factor eIF-4F suggest a role in translational control. Heat shock effects on eIF-4F, J. Biol. Chem. 262 (1987) 380–388.
[7] H.G. Wendel, R.L.A. Silva, A. Malina, J.R. Mills, H. Zhu, T. Ueda, R. Watanabe-Fukunaga, R. Fukunaga, J. Teruya-Feldstein, J. Pelletier, Dissecting eIF4E action in tumorigenesis, Genes Dev. 21 (2007) 3232–3237.
[8] H.G. Wendel, E. De Stanchina, J.S. Fridman, A. Malina, S. Ray, S. Kogan, C. Cordon-Cardo, J. Pelletier, S.W. Lowe, Survival signalling by Akt and eIF4E in oncogenesis and cancer therapy, Nature 428 (2004) 332–337.
[9] A.J. Waskiewicz, A. Flynn, C.G. Proud, J.A. Cooper, Mitogen-activated protein kinases activate the serine/threonine kinases Mnk1 and Mnk2, EMBO J. 16 (1997) 1909–1920.
[10] L. Furic, L. Rong, O. Larsson, I.H. Koumakpayi, K. Yoshida, A. Brueschke, E. Petroulakis, N. Robichaud, M. Pollak, L.A. Gaboury, eIF4E phosphorylation promotes tumorigenesis and is associated with prostate cancer progression, Proc. Natl. Acad. Sci. U. S. A. 107 (2010) 14134–14139.
[11] T. Ueda, M. Sasaki, A.J. Elia, I.I.C. Chio, K. Hamada, R. Fukunaga, T.W. Mak, Combined deficiency for MAP kinase-interacting kinase 1 and 2 (Mnk1 and Mnk2) delays tumor development, Proc. Natl. Acad. Sci. U. S. A. 107 (2010) 13984–13990.
[12] T. Ueda, R. Watanabe-Fukunaga, H. Fukuyama, S. Nagata, R. Fukunaga, Mnk2 and Mnk1 are essential for constitutive and inducible phosphorylation of eukaryotic initiation factor 4E but not for cell growth or development, Mol. Cell. Biol. 24 (2004) 6539–6549.
[13] J. Bain, L. Plater, M. Elliott, N. Shpiro, C.J. Hastie, H. McLauchlan, I. Klevernic, J.S.C. Arthur, D.R. Alessi, P. Cohen, The selectivity of protein kinase inhibitors: a further update, Biochem. J. 408 (2007) 297–315.
[14] A. Sussman, et al., Discovery of cercosporamide, a known antifungal natural product, as a selective Pkc1 kinase inhibitor through high-throughput screening, Eukaryot. Cell 3 (2004) 932–943.
[15] B.W. Konicek, et al., Therapeutic inhibition of MAP kinase interacting kinase blocks eukaryotic initiation factor 4E phosphorylation and suppresses outgrowth of experimental lung metastases, Cancer Res. 71 (2011) 1849–1857.
[16] S. Diab, T. Teo, M. Kumarasiri, P. Li, M. Yu, F. Lam, S.K. Basnet, M.J. Sykes, H. Albrecht, R. Milne, S. Wang, Discovery of 5-(2-(phenylamino)pyrimidin-4-yl)thiazol-2(3H)-one derivatives as potent Mnk2 inhibitors: synthesis, SAR analysis and biological evaluation, ChemMedChem 9 (2014) 962–972.
[17] F.M. Balis, Evolution of anticancer drug discovery and the role of cell-based screening, J. Natl. Cancer Inst. 94 (2002) 78–79.
[18] R. Jauch, S. Jakel, C. Netter, K. Schreiter, B. Aicher, H. Jackle, M.C. Wahl, Crystal structures of the Mnk2 kinase domain reveal an inhibitory conformation and a zinc binding site, Structure 13 (2005) 1559–1568.
[19] J. Hou, T. Teo, M.J. Sykes, S. Wang, Insights into the importance of DFD-motif and insertion I1 in stabilizing the DFD-out conformation of Mnk2 kinase, ACS Med. Chem. Lett. 4 (2013) 736–741.
[20] R. Jauch, M.K. Cho, S. Jakel, C. Netter, K. Schreiter, B. Aicher, M. Zweckstetter, H. Jackle, M.C. Wahl, Mitogen-activated protein kinases interacting kinases are autoinhibited by a reprogrammed activation segment, EMBO J. 25 (2006) 4020–4032.

[21] J. Oyarzabal, N. Zarich, M.I. Albarran, I. Palacios, M. Urbano-Cuadrado, G. Mateos, I. Reymundo, O. Rabal, A. Salgado, A. Corrionero, J.s. Fominaya, J. Pastor, J.R. Bischoff, Discovery of mitogen-activated protein kinase-interacting kinase 1 inhibitors by a comprehensive fragment-oriented virtual screening approach, J. Med. Chem. 53 (2010) 6618–6628.
[22] K. Slentz-Kesler, J.T. Moore, M. Lombard, J. Zhang, R. Hollingsworth, M.P. Weiner, Identification of the human Mnk2 gene (MKNK2) through protein interaction with estrogen receptor beta, Genomics 69 (2000) 63–71.
[23] G.C. Scheper, N.A. Morrice, M. Kleijn, C.G. Proud, The mitogen-activated protein kinase signal-integrating kinase Mnk2 is a eukaryotic initiation factor 4E kinase with high levels of basal activity in mammalian cells, Mol. Cell. Biol. 21 (2001) 743–754.
[24] J.L. Parra, M. Buxade, C.G. Proud, Features of the catalytic domains and C termini of the MAPK signal-integrating kinases Mnk1 and Mnk2 determine their differing activities and regulatory properties, J. Biol. Chem. 280 (2005) 37623–37633.
[25] S. Joshi, L.C. Platanias, Mnk kinases in cytokine signaling and regulation of cytokine responses, Biomol. Concepts 3 (2012) 127–139.
[26] J. Bostrom, J.R. Greenwood, J. Gottfries, Assessing the performance of OMEGA with respect to retrieving bioactive conformations, J. Mol. Graph. Model 21 (2003) 449–462.
[27] M. McGann, FRED pose pediction and virtual screening accuracy, J. Chem. Inf. Model 51 (2011) 578–596.
[28] C. Tschopp, U. Knauf, M. Brauchle, M. Zurini, P. Ramage, D. Glueck, L. New, J. Han, H. Gram, Phosphorylation of eIF-4E on Ser 209 in response to mitogenic and inflammatory stimuli is faithfully detected by specific antibodies, Mol. Cell Biol. Res. Commun. 3 (2000) 205–211.
[29] J.A. Grant, M.A. Gallardo, B.T. Pickup, A fast method of molecular shape comparison: a simple application of a Gaussian description of molecular shape, J. Comput. Chem. 17 (1996) 1653–1666.
[30] S. Lapenna, A. Giordano, Cell cycle kinases as therapeutic targets for cancer, Nat. Rev. Drug Discov. 8 (2009) 547–566.
[31] V. Dulic, W.K. Kaufmann, S.J. Wilson, T.D. Tlsty, E. Lees, J.W. Harper, S.J. Elledge, S.I. Reed, p53-dependent inhibition of cyclin-dependent kinase activities in human fibroblasts during radiation-induced G1 arrest, Cell 76 (1994) 1013–1023.
[32] F. Lam, A.Y. Abbas, H. Shao, T. Teo, J. Adams, P. Li, T.D. Bradshaw, P.M. Fischer, E. Walsby, C. Pepper, Y. Chen, J. Ding, S. Wang, Targeting RNA transcription and translation in ovarian cancer cells with pharmacological inhibitor CDKI-73, Oncotarget 5 (2014) 7691–7704.
[33] H. Quentmeier, J. Reinhardt, M. Zaborski, H.G. Drexler, FLT3 mutations in acute myeloid leukemia cell lines, Leukemia 17 (2003) 120–124.
[34] E.R. Sharlow, S. Leimgruber, A. Yellow-Duke, R. Barrett, Q.J. Wang, J.S. Lazo, Development, validation and implementation of immobilized metal affinity for phosphochemicals (IMAP)-based high-throughput screening assays for low-molecular-weight compound libraries, Nat. Protoc. 3 (2008) 1350–1363.
[35] M. Koresawa, T. Okabe, High-throughput screening with quantitation of ATP consumption: a universal non-radioisotope, homogeneous assay for protein kinase, Assay. Drug Dev. Technol. 2 (2004) 153–160.
[36] H. Shao, S. Shi, S. Huang, A.J. Hole, A.Y. Abbas, S. Baumli, X. Liu, F. Lam, D.W. Foley, P.M. Fischer, M. Noble, J.A. Endicott, C. Pepper, S. Wang, Substituted 4-(thiazol-5-yl)-2-(phenylamino)pyrimidines are highly active CDK9 inhibitors: synthesis, X-ray crystal structures, structure-activity relationship, and anticancer activities, J. Med. Chem. 56 (2013) 640–659.
[37] T. Lehmann-Lintz, J. Kley, N. Redemann, A. Sauer, L. Thomas, D. Wiedenmayer, M. Austen, J. Danilewicz, M. Schneider, K. Schreiter, P. Black, W. Blackaby, and I. Linney, WO 2011/104337 A1, 2011.
[38] VIDA, Version 4.0.3, Openeye Scientific Software, Sante Fe, NM, 2010.
[39] OEDocking, Version 3.0.0, Openeye Scientific Software, Sante Fe, NM, 2012.
[40] ROCS, Version 3.1.2, Openeye Scientific Software, Sante Fe, NM, 2011.
[41] Babel, Version 3.3, Openeye Scientific Software, Sante Fe, NM, 2007.
[42] FILTER, Version 2.1.1, Openeye Scientific Software, Sante Fe, NM, 2010.
[43] OMEGA, Version 2.4.6, Openeye Scientific Software, Sante Fe, NM, 2012.
[44] G.B. McGaughey, R.P. Sheridan, C.I. Bayly, J.C. Culberson, C. Kreatsoulas, S. Lindsley, V. Maiorov, J.F. Truchon, W.D. Cornell, Comparison of topological, shape, and docking methods in virtual screening, J. Chem. Inf. Model 47 (2007) 1504–1519.
[45] M.J. Sykes, R.A. McKinnon, J.O. Miners, Prediction of metabolism by cytochrome P450 2C9: alignment and docking studies of a validated database of substrates, J. Med. Chem. 51 (2008) 780–791.
[46] A.B. Reitz, E.W. Baxter, E.E. Codd, C.B. Davis, A.D. Jordan, B.E. Maryanoff, C.A. Maryanoff, M.E. McDonnell, E.T. Powell, M.J. Renzi, M.R. Schott, M.K. Scott, R.P. Shank, J.L. Vaught, Orally active benzamide antipsychotic agents with affinity for dopamine D2, serotonin 5-HT1A, and adrenergic alpha1 receptors, J. Med. Chem. 41 (1998) 1997–2009.
[47] P. Burkhard, U. Hommel, M. Sanner, M.D. Walkinshaw, The discovery of steroids and other novel FKBP inhibitors using a molecular docking program, J. Mol. Biol 287 (1999) 853–858.
[48] D.B. Jordan, G.S. Basarab, D.I. Liao, W.M. Johnson, K.N. Winzenberg, D.A. Winkler, Structure-based design of inhibitors of the rice blast fungal enzyme trihydroxynaphthalene reductase, J. Mol. Graph. Model 19 (2001) 434–447, 470-431.
[49] J.W. Liebeschuetz, S.D. Jones, P.J. Morgan, C.W. Murray, A.D. Rimmer, J.M. Roscoe, B. Waszkowycz, P.M. Welsh, W.A. Wylie, S.C. Young, H. Martin, J. Mahler, L. Brady, K. Wilkinson, PRO_SELECT: combining structure-based drug design and array-based chemistry for rapid lead discovery. 2. The development of a series of highly potent and selective factor Xa inhibitors, J. Med. Chem 45 (2002) 1221–1232.
[50] H. Park, H. Choi, S. Hong, S. Hong, Identification of novel BRAF kinase inhibitors with structure-based virtual screening, Bioorg. Med. Chem. Lett 21 (2011) 5753–5756.
[51] T. Teo, M. Yu, Y. Yang, T. Gillam, F. Lam, M.J. Sykes, S. Wang, Pharmacologic co-inhibition of Mnks and mTORC1 synergistically suppresses proliferation and perturbs cell cycle progression in blast crisis-chronic myeloid leukemia cells, Cancer Lett 357 (2015) 612–623.
[52] M. Yu, P. Li, S.K.C. Basnet, M. Kumarasiri, S. Diab, T. Teo, H. Albrecht, S. Wang, Discovery of 4-(dihydropyridinon-3-yl)amino-5-methylthieno[2,3-d]pyrimidine derivatives as potent Mnk inhibitors: synthesis, structure-activity relationship analysis and biological evaluation, Eur. J. Med. Chem 95 (2015) 116–126.
[53] T. Teo, F. Lam, M. Yu, Y. Yang, S.K. Basnet, H. Albrecht, M.J. Sykes, S. Wang, Pharmacologic inhibition of MNKs in acute myeloid leukemia, Mol. Pharmacol 88 (2015) 380–389.
[54] Y. Cheng, W.H. Prusoff, Relationship between the inhibition constant (K1) and the concentration of inhibitor which causes 50 per cent inhibition (I50) of an enzymatic reaction, Biochem. Pharmacol 22 (1973) 3099–3108.